

Effect of the Curvature Angle in a Conduit with an Adiabatic Cylinder over a Backward Facing Step on the Magnetohydrodynamic Behaviour in the Presence of a Nanofluid

Djamila Derbal^{1,*} – Mohamed Bouzit¹ – Abderrahim Mokhefi² – Fayçal Bouzit¹

¹ University of Science and Technology of Oran, Faculty of Mechanical , Algeria

² Bechar University, Faculty of Sciences and Technology, Algeria

A backward facing duct are present in various industrial applications especially those focused on heat transfer. The flow through a curved backward facing duct especially in the presence of nanofluid presents complexities compared to a straight backward facing step (BFS) duct. Therefore, the present numerical study deals a nanofluid flow ($Fe_3O_4-H_2O$) forced convection in a curved backward facing duct. The objective of this investigation is to visualize at different curvature angles g (0° , 30° , 45° , 60° , 90°) imposed on the top wall of the duct, the effect of Hartmann number Ha (0 , 50 , 100), magnetic field inclination angle γ (0° , 60° , 90°), Reynolds number Re (10 , 100 , 200) and nanoparticle volume fraction ϕ (0% , 0.05% , 0.1%). The dimensionless governing equations are solved using the multigrid finite element method. The results showed that the heat transfer was enhanced at the curved angle $g = 90^\circ$ for large Hartman numbers, thus, the average Nusselt number increased with a ratio of 240.74% in the case of Hartmann number ($Ha = 100$).

Keywords: forced convection, backward-facing step, curved conduit, fixed cylinder, ferrofluid, finite element method, magnetohydrodynamic

Highlights

- The discussion of magnetohydrodynamic behavior of laminar ferrofluid flow through a curved backward facing duct with a fixed cylinder is presented.
- The use of the horizontal magnetic field in the case of a curved geometry provide an enhancement of the heat transfer. Indeed, we note an increase of about 240% in the heat transfer rate in case of important magnetic flux density.
- In the case of a curved backward facing duct, the presence of a vertical magnetic field has no effect on heat transfer.
- The increase in Reynolds number, Hartmann number and volume fraction of the nanoparticles enhance the heat transfer through a curved backward facing duct.

0 INTRODUCTION

The sudden expansion geometry in a duct creates a separation and reattachment of the flow, as this expansion is a determining factor in the structure of the flow so the heat transfer is significantly affected. Thus, this geometry has a very important role in various engineering applications such as gas turbine engines, heat exchangers, combustion chambers, aircraft, and electronic devices and around buildings and many others. Indeed, it is receiving a lot of attention, so many studies focused on the separation and reattachment of the flow backward-facing step. For important Reynolds numbers Erturk [1] investigated a simulation of incompressible laminar steady flow in two dimensions (2D). In three-dimensional (3D), Lan et al. [2] presented in rectangular duct, a numerical study of laminar forced convection flow by means of a $K-\epsilon-\zeta-f$ turbulence model. Iwai et al. [3] presented at little Reynolds number, the effect of the duct aspect ratio. An agreement of the numerical results with

experimental results was revealed. Moreover, an increase of the Nusselt number near the sidewalls in the cases studied. Star et al. [4] developed for different Richardson number a reduced-order proper orthogonal decomposition (POD)-Galerkin simulation Reynolds-averaged Navier–Stokes (RANS) extended to low Prandtl number flow. In the fact, the buoyancy marks its influence on flow and heat transfer. In addition to a more accurate prediction of the flow behavior, the description of the fluid parameters as well as the identification of the rheological consequences are interesting. Kahine et al. [5] demonstrated the stabilizing impact of the shear thinning character of the fluid by numerical simulation compared to experimental data. To represent Newtonian fluids and the power law relationship between viscosity and shear rate, Mahmood et al. [6] analyzed the flow of Newtonian materials and a power law fluid representing the characteristics of shear thinning, thickening, with the finite element method. The control of turbulent flows can be realized using either

*Corr. Author's Address: University of Science and Technology of Oran, Faculty of Mechanical Eng., Maritime Science and Eng., Algeria, djamila.derbal@univ-usto.dz

external, stable or unstable forcing, and is of basic as well as practical interest [7]. Benard et al. [8] and Li et al. [9] studied the effect of periodic perturbations with an imposed frequency and amplitude on the evolution of vortices formed downstream of a backward facing step (BFS). For the little Reynolds number, Koide et al. [10] to enhance heat transfer; they provided a numerical simulation based on experimental data, behind a backward facing step, on the flow attachment in the transient regime. Tihon et al. [11] evaluated the effects of various control parameters on the periodic disturbance introduced in the flow. They presented an experimental approach, to examine the flow behavior in the backward flow step by means of the fluctuating wall shear rate downstream of the step, as well as the effect of the inlet flow pulses on the overall flows structure.

Heat transfer is the concern of many researches, so its improvement according to the process needs. A new method has been introduced to intensify the convective heat transfer, is to inject nanoparticles into the base fluid. In this regard, several recent researches have been carried out to show the effectiveness of using these nanoparticles in base fluids. The addition of nanoparticles in the base fluid marks their significant effect in different processes particularly those that concentrate on the thermal transfer [12] to [14]. Selimefendigil et al. [15] studied the effects of nanoparticles volume fraction, the inlet oscillation frequency and the Reynolds number on the fluid flow and thermal transfer features. They showed that the heat transfer is increased with the enhancement of the volume fraction of the nanoparticles, the Reynolds number and the frequency of the oscillation, experimentally, the degree of heat transfer flow over a backward-facing step duct increases as the volume concentration of the nanoparticles increases [16]. In order to observe clearly the effect of expanding rate, Togun et al. [17] introduces a numerical simulation of a turbulent and laminar heat transfer flow of nanofluid on a backward step, and various control parameters assumed. The results reveal that the angle of incidence of the vortex generators has significant effects on the heat transfer increase. Ahmed et al. [18] examined the forced convection heat transfer of a laminar fluid flow on a microscale BFS, the result indicates that the heat transfer is enhanced with a little increase in pressure drop in the case of a rectangular vortex generator (VG) wing with an angle of attack of 60° and a Reynolds number of 180. Abbassi and Nassrallah [19] analyzed the laminar flow of a viscous incompressible nanofluid through a backward-facing step duct under the effect of a magnetic field. They discussed the

magneto hydrodynamic behavior under the effect of some control parameters. Furthermore, they demonstrated that the magnetic field significantly improves the heat transfer at high Prandtl numbers. Kumar and Dhiman [20] investigated for a particular Prandtl number and at different values of Re the forced convection characteristics of backward laminar flow in a two-dimensional channel. They discussed the effect of cylinder position on flow and heat transfer, an enhancement of the Nusselt number while using a circular cylinder compared to the case without a cylinder. Hussain et al. [21] we applied the Galerkin finite element method to compute the forced convective flow of a ferrofluid within a BFS containing a rotating cylinder with a fixed diameter. The magneto hydrodynamic behavior was analyzed assuming a wide range of control parameters namely Reynolds number, Hartmann number, magnetic field inclination angle and nanoparticle volume fraction. The effect of these parameters on the thermo magnetohydrodynamic (MHD) structure has been demonstrated. In addition, Selimefendigil and Öztop [22] presented the impact of these parameters on the flow and on the heat transfer in the case of mixed convection through a duct without cylinder. Mohammed et al. [23] investigated numerically, the effects on hydrodynamic and heat transfer of four different types of shapes that block the mixed convective of the laminar transient nanofluid flow through microscale BFS placed in a horizontal duct. Kherbeet et al. [24] showed the heat transfer characteristics reported experimentally and numerically on a laminar convective flow using a nanofluid with two nanoparticles types. It has been, shown that the Nusselt number increases and improves in the case of one nanofluid over the other. Lv et al. [25] in two-dimensional backward step flow, based on the analysis of several parameters, the flow characteristics are studied quantitatively using particle image velocimetry (PIV) while changing the Reynolds number and the weight nanofluid fraction. The mass and momentum transfer in the nanofluid improved, which leads to an improvement of the heat transfer. Amiri et al. [26] added an experimental study on the thermo-physical properties of egg nucleoplasm (EggNP). The results indicate that a greater weight nanofluid concentration involves a faster rate of heat transfer on a backward facing step. Niemann and Fröhlich [27] in a turbulent mixed convective flow, they studied the buoyancy effect on the velocity field and on heat transfer is by comparing two simulations, one with the buoyancy term removed from the equations, and the other with a Richardson number of

0.338. The results contribute to the physical understanding of the effects of buoyancy on heat transfer in the considered regime. In addition, the data generated provides validation and improvement of turbulence models for turbulent heat transfer at low Prandtl numbers. To show the fin's impact on heat transfer, Boruah et al. [28] investigated the thermal-hydrodynamic properties and entropy creation for a mixed convective flow across a channel BFS with various baffle geometries. The results indicate that the wedge-shaped elliptical baffle arrangement in the duct BFS is an ideal design from the point of view of thermal-hydraulic efficiency and entropy generation. Thermal-hydrodynamic characteristics of fluids flowing through downward flowing duct in the presence of obstacles have received relatively little attention in the literature, despite the important effect that these obstacles can have on the flow structure and heat transfer [29]. Selimefendigil and Öztöp [30] studied numerically the forced convection heat transfer over a backward facing step duct with a baffle on the top wall on a pulsating laminar flow. The effects of several important parameters were discussed, compared to a steady flow without baffle. They showed that in the case of a lower wall downstream of the enlargement, the presence of a deflector is not beneficial for the improvement of heat transfer. Selimefendigil and Öztöp [31] studied numerically the laminar forced convection of a pulsed nanofluid flow over a BFS. They treated the effect of several control parameters and different geometrical factors namely: length and height of the bottom wall surface corrugation. The results show that the rate heat transfer increases with the inclusion of nanoparticles. Moreover, the rate of enhancement depends on the volume fraction of nanoparticles in the base fluid. Boruah et al. [32] demonstrated numerically a mixed convection flow of an incompressible non-Newtonian fluid across a channel BFS with a chicane. The results showed the impact of baffle location and nanoparticle diameter on the convective transfer. Furthermore, these results are beneficial for the design of a thermodynamic system capable of achieving maximum heat transfer with minimum irreversibility. Mohammed et al. [33] have numerically simulated a mixed convection flows of laminar and turbulent nanofluid on a backwards step. They analyzed the effect of geometrical parameters such as height, position of baffles, width and number of baffles analyzed. Heshmati et al. [34] presented the effect of several control parameters as well as deflectors with four different geometries. In addition, the effect of inclination and location was included. Due to the

importance of thermal phenomena in curved ducts, several researches have been conducted in the literature. In order to give a detailed knowledge, to understand the complexity of non-isothermal flows, to prevent the phenomena of hydrodynamic instability that can occur, researchers have carried out work on non-isothermal flows to highlight these phenomena in this type of duct. Yanase et al. [35] proposed a numerical simulation of the convective non-isothermal heat transfer flow through a curved rectangular duct. The calculations performed by the spectral method for different Grashof numbers and Dean numbers. Several satisfactory results are obtained in terms of velocity and temperature. In addition, the convection remarkably enhanced from the hot wall to the fluid. Mondal et al. [36] studied numerically a convective heat transfer flow through a curved duct. Therefore, they treated the effect of Grashof number and aspect ratio on the thermo-hydrodynamic flow behavior over a wide temperature difference range applied to the cold inside and hot outside. Li et al. [37] presented a combination of experimental and numerical study to demonstrate the three-dimensional behavior of laminar flow in 120° curved rectangular ducts with three aspect ratios (Ar) and continuous curvature variation (Cr). The results show the complex changes in the formation, evolution of Dean vortices of different types. Furthermore, they demonstrated the effect of these control parameters on the instability of Dean vortices in the case of turbulent flow. Choi and Park [38] studied numerically the mixed convection flows through curved concentric annular ducts with constant wall temperature. The simulation was performed for different Dean numbers, different Grashof numbers and different radius ratios. Indeed, they presented the effect of these control parameters. Furthermore, they showed that for the Grashof number critical value, the average Nusselt number showed a strong dependence on the Dean number and the radius ratio. Chandratilleeke et al. [39] presented a numerical study to examine the development of recirculation zones and the appropriate heat transfer phenomenon that takes place from a laminar fluid flow through curved rectangular duct. In fact, they carefully analyzed the flow conditions leading to hydrodynamic instability and the generation of Dean vortices in curved duct, identifying the influences of the different control parameters. In addition, they examined the buoyancy force effect and secondary flow on the thermal process. Choi and Zhang [40] carried out a numerical simulation to evaluate the forced convection of a laminar flow of Al_2O_3 nanofluid through a curved duct. They found that the addition of Al_3O_2

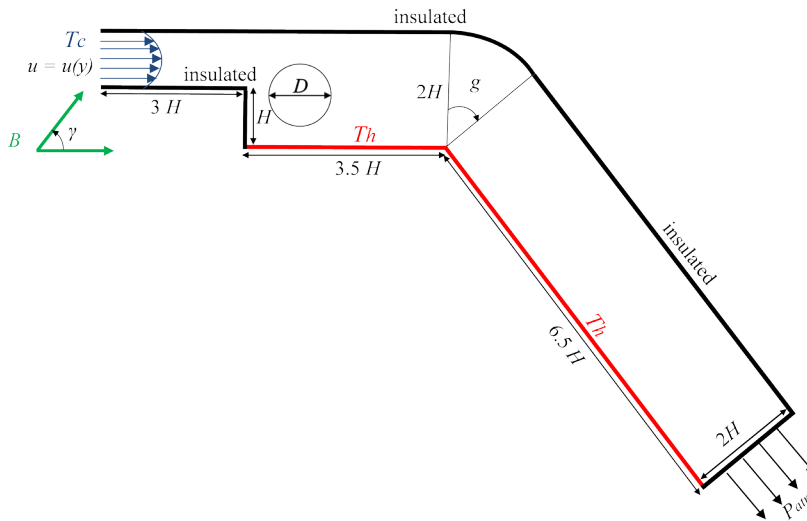


Fig. 1. The physical configuration with the boundary conditions

nanoparticles at low and increasing concentrations increases the average Nusselt number. Ajeel et al. [41] showed that different control parameters such as the corrugated shape of the curved duct, the installation of baffles with different geometric ratios as well as the hybridization of the nanoparticles positively affect the heat transfer.

The analysis of various previous works has shown that the thermo-magneto-hydrodynamic behavior in curved duct has not been widely studied especially the one with backward-facing step and in the presence of nanoparticles. In this regard, the objective of the present study is to provide a numerical simulation of a forced laminar convective flow, in the presence of Fe₃O₄ nanoparticles in the base fluid (water), through a curved backward-facing step duct containing a fixed adiabatic cylinder under an inclined magnetic field and using a single-phase nanofluid model. The finite element method was used to solve the equations governing the considered fluid flow. The influence of the curvature angle on the thermal and hydrodynamic structures was demonstrated for different values of the several control parameters.

1 GEOMETRIC DESCRIPTION

The physical study presentation, consists of a curved backward facing duct, containing a fixed cylinder of diameter D , centrally located at $(4H, H)$, see (Fig. 1). In addition, an angle of curvature (g) is imposed on the duct and an external magnetic field has been imposed at an angle (γ). The expansion ratio is set to 2 and the step height is taken as H , halfway up the duct. The

effects of viscous dissipation and Joule heating are not taken in to account the energy equation modelling. The induced magnetic field was assumed negligible. The ferrofluid at the inlet T_c , on the other hand, the bottom wall downstream of the step is maintained at a high temperature T_h and the other walls are maintained thermally adiabatic. The water and iron oxide thermo physical properties are presented in Table 1. The physical situation with boundary conditions is presented in Fig. 1.

Table 1. Thermophysical properties of water (H₂O) and iron oxide nanoparticles [21]

Physical properties	Water (H ₂ O)	Nanoparticles (Fe ₃ O ₄)
Density [kg·m ⁻³]	997.1	5,200.0
Specific heat [J·kg ⁻¹ ·K ⁻¹]	4,179	670.0
Thermal conductivity [W·m ⁻¹ ·K ⁻¹]	0.613	6.0000
Thermal expansion [K ⁻¹] ($\times 10^{-5}$)	0.613	1.1800
Electrical conductivity [S·m ⁻¹]	0.050	25,000

2 MATHEMATICAL MODEL

2.1 Governing Equations

$$\frac{\partial u}{\partial x} + \frac{\partial v}{\partial y} = 0, \tag{1}$$

$$\rho_{ff} \left(u \frac{\partial u}{\partial x} + v \frac{\partial u}{\partial y} \right) = -\frac{\partial p}{\partial x} + \mu_{ff} \left(u \frac{\partial^2 u}{\partial x^2} + v \frac{\partial^2 u}{\partial y^2} \right) + \sigma_{ff} B_0^2 (v \sin \gamma \cos \gamma - u \sin^2 \gamma), \tag{2}$$

$$\rho_{ff} \left(u \frac{\partial v}{\partial x} + v \frac{\partial u}{\partial y} \right) = -\frac{\partial p}{\partial y} + \mu_{ff} \left(u \frac{\partial^2 v}{\partial x^2} + v \frac{\partial^2 v}{\partial y^2} \right) + \sigma_{ff} B_0^2 (u \sin \gamma \cos \gamma - v \cos^2 \gamma), \quad (3)$$

$$u \frac{\partial T}{\partial x} + v \frac{\partial T}{\partial y} = \alpha_{ff} \left(\frac{\partial^2 T}{\partial x^2} + \frac{\partial^2 T}{\partial y^2} \right). \quad (4)$$

The following equation present the stream function:

$$\frac{\partial \psi}{\partial x} = -v, \quad \frac{\partial \psi}{\partial y} = u. \quad (5)$$

2.2 Boundary conditions

For the numerical calculation of this study situation, the imposed boundary conditions are expressed as follows:

- Input condition: a parabolic velocity profile in the direction of the x -axis and a uniform cold temperature:

$$u = u(y), \quad v = 0, \quad T = T_c. \quad (6)$$

- At the bottom wall downstream of the expansion: The conditions of no-slip velocity and uniform hot temperature:

$$u = v = 0, \quad T = T_h. \quad (7)$$

- Outlet condition: The gradient of velocity and temperature in the normal direction (normal direction coincide with x -axis):

$$\frac{\partial u}{\partial n} = \frac{\partial v}{\partial n} = 0, \quad \frac{\partial T}{\partial n} = 0. \quad (8)$$

- The no-slip boundary conditions for the velocity are applied on the duct walls and on the cylinder contour and the adiabatic conditions for the temperature are imposed except for the bottom hot wall downstream of the expansion:

$$u = v = 0, \quad \frac{\partial T}{\partial n} = 0. \quad (9)$$

2.3 Dimensionless Governing Equations

To transform the set of partial differential equations into a dimensionless form, the following variables given in Table 2 were used. The boundary conditions used in the dimensionless form are summarized in Table 3. The thermo-physical properties of the ferrofluid are depend on the properties of the base fluid and the magnetic nanoparticles. Hence, the

effective thermo-physical properties of the nanofluid are given above in Table 4.

Table 2. The variables used to transform the system of partial differential equations in to dimensionless form

$X = \frac{x}{H},$	$U = \frac{u}{u},$	$P = \frac{p}{\rho_{ff} u^2}$
$Y = \frac{y}{H}$	$V = \frac{v}{u}$	
	$Pr = \frac{\nu_f}{\alpha_{ff}},$	
$\theta = \frac{T - T_c}{T_h - T_c}$	$Re = \frac{H u}{\nu_f}$	$Ha = B_0 H \sqrt{\frac{\sigma_{ff}}{u_{ff}}}$

The dimensionless equations governing the flow summarized as follows:

$$\frac{\partial U}{\partial X} + \frac{\partial V}{\partial X} = 0, \quad (10)$$

$$U \frac{\partial U}{\partial X} + V \frac{\partial U}{\partial Y} = -\frac{\partial P}{\partial X} + \frac{1}{Re} \frac{u_{ff}}{\rho_{ff} \nu_f} \left(\frac{\partial^2 U}{\partial X^2} + \frac{\partial^2 U}{\partial Y^2} \right) + \frac{\rho_f \sigma_{ff} Ha^2}{\rho_{ff} \sigma_f Re} (V \sin \gamma \cos \gamma - U \sin^2 \gamma), \quad (11)$$

$$U \frac{\partial V}{\partial X} + V \frac{\partial V}{\partial Y} = -\frac{\partial P}{\partial Y} + \frac{1}{Re} \frac{u_{ff}}{\rho_{ff} \nu_f} \left(\frac{\partial^2 V}{\partial X^2} + \frac{\partial^2 V}{\partial Y^2} \right) + \frac{\rho_f \sigma_{ff} Ha^2}{\rho_{ff} \sigma_f Re} (U \sin \gamma \cos \gamma - V \cos^2 \gamma), \quad (12)$$

$$U \frac{\partial \theta}{\partial X} + V \frac{\partial \theta}{\partial Y} = \frac{1}{Re Pr} \frac{\alpha_{ff}}{\alpha_f} \left(\frac{\partial^2 \theta}{\partial X^2} + \frac{\partial^2 \theta}{\partial Y^2} \right). \quad (13)$$

The dimensionless equations stream function given as follows:

$$\frac{\partial \Psi}{\partial X} = -V, \quad \frac{\partial \Psi}{\partial Y} = U. \quad (14)$$

2.4 The Local and Nu_{ave} Number

A convective heat transfer occurred due to the difference temperature between the flowing nanofluid and the hot wall downstream of the expansion. This heat flow can be estimated using the Nusselt number. This local dimensionless number is defined as a thermal gradient over the heated surface. In effect, it gives a measure of the convective heat transfer that occurs on that surface.

Table 3. Boundary conditions introduced in dimensionless form

At the channel inlet:	$U = U(y), \quad V = 0, \quad \theta = 0, \quad \frac{\partial \Psi}{\partial Y} = 1$
At the downstream bottom wall:	$U = 0, \quad V = 0, \quad \theta = 1, \quad \frac{\partial \Psi}{\partial X} = 0$
At the channel outlet:	$\frac{\partial U}{\partial X} = \frac{\partial V}{\partial X} = \frac{\partial \theta}{\partial X} = 0, \quad \frac{\partial \Psi}{\partial Y} = U_s$
On the channel walls (except the bottom wall):	$U = V = \frac{\partial \theta}{\partial n} = 0, \quad \Psi = 0$
On the boundary of cylinder:	$U = V = 0, \quad \frac{\partial \theta}{\partial n} = 0, \quad \Psi = 0$

Table 4. The effective thermo-physical characteristics of the nanofluid

Density:	$\rho_{ff} = (1-\varphi)\rho_f + \varphi\rho_s$
Thermal diffusivity:	$\alpha_{ff} = \frac{K_{ff}}{(\rho c_p)_{ff}}$
Electrical conductivity:	$\sigma_{ff} = \sigma_f \left(1 + \frac{3(\sigma-1)\varphi}{(\sigma+2) - (\sigma-1)\varphi} \right), \sigma = \frac{\sigma_s}{\sigma_f}$
Specific heat:	$(\rho c_p)_{ff} = (1-\varphi)(\rho c_p)_f + \varphi(\rho c_p)_s$
Thermal expansion coefficient:	$(\rho\beta)_{ff} = (1-\varphi)(\rho\beta)_f + \varphi(\rho\beta)_s$
Thermal conductivity:	$\frac{k_{ff}}{k_f} = \frac{k_s + 2k_f - 2\varphi(k_f - k_p)}{k_s + 2k_f + \varphi(k_f - k_p)}$
Dynamic viscosity:	$\mu_{ff} = \frac{\mu_f}{(1-\varphi)^{2.5}}$

The local Nusselt number on the heated wall is defined as follows:

$$Nu = \frac{h_{ff}H}{k_f}, \tag{15}$$

where h_{ff} is the heat transfer coefficient represented as follows:

$$h_{ff} = \frac{q_w}{T_h - T_c}, \tag{16}$$

where q_w stands the heat flux on the heated wall given as follows:

$$q_w = -k_{ff} \frac{T_h - T_c}{H} \frac{\partial \theta}{\partial n} \Big|_{L_1+l}. \tag{17}$$

We substitute Eq. (17) into Eq. (16) and Eq. (16) into Eq. (15); we will have the following result:

$$Nu = \frac{k_{ff}}{k_f} \frac{\partial \theta}{\partial n}. \tag{18}$$

The Nusselt number given by integrating the local Nusselt along the length of the hot wall as follows:

$$Nu_{ave} = \frac{1}{L_1+l} \left(\int_0^{L_1} Nu \, dx + \int_0^l Nu \, dl \right), \tag{19}$$

where L_1 represent the horizontal length part hot wall, l represent the inclined length part hot wall.

3 VALIDATION CODE AND GRID INDEPENDENCE TEST

The general solving procedure focuses on numerical methods. The discretization of the governing equations consists in transforming the differential form of the governing systems Eqs. (10) to (14) into a discrete algebraic form that defines all unknowns at each point of a used grid. The finite element method based on Galerkin discretization is implemented to solve the present problems because of its flexibility for complex geometries through different types of meshes on the one hand, and the ease of introducing boundary conditions in the form of flows on the other hand. The application of the present method requires a rewriting of the governing equations in integral form. The weak formulation is used to include the boundary conditions. The numerical solution goes through the following steps: introduction of the mesh, approximation of the dependent functions, assembly and application of the boundary conditions and finally the solution of the global system of equations. The mesh adopted for the present study, shown in Fig. 2, has in its entirety a triangular shape. It is refined near the duct walls and near the cylinder circumference. However, an unstructured triangular mesh has been introduced in the rest of the duct. It should be noted that near the duct walls and near the cylinder circumference, a rectangular boundary layer mesh was used to ensure that the grid presentation is well aligned with the flow. In each node of the defined grid, to complete the computation in terms of iteration number, the convergence criterion used consists in stopping the calculation when the absolute difference between the old and the new values of the dependent variables, namely U, V, P and θ becomes less than 10^{-6} . If Ψ and n present respectively a dependent variable and iteration order, this criterion is established using the following formula:

$$\left| \frac{\Psi^{n+1} - \Psi^n}{\Psi^{n+1}} \right| < 10^{-6}. \quad (20)$$

The results obtained from the computational code should be independent of the grid form and not be modified by increasing the mesh elements number. Therefore, different grids were verified. Table 5 gives the evolution of the average Nusselt number, the dimensionless mean temperature and the dimensionless temperature for different numbers of mesh elements that were considered in the present simulation. The verification of the mesh was carried out for the case $g = 90^\circ$ at $Pr = 6.2$, $Re = 300$, $Ha = 0$, $\gamma = 0^\circ$, $\varphi = 0.05$. We have chosen to use a mesh corresponding to a number of elements equal to 41401 beyond which there was no change in terms of average Nusselt number, mean and local dimensionless temperature. To confirm the accuracy of these numerical results, validation with other previous work is necessary. The numerical results of this work were compared with the numerical results of Hussain and Ahmed [18]. They numerically studied the forced convection of a laminar flow of a ferrofluid around a cylinder inside a backward facing step. Therefore, the isotherm forms obtained in the present work were compared with the results of the reference mentioned above, see Fig. 4, this comparison was done in the case of $Ha = 0$ and $Ha = 100$ for values of $Pr = 6.2$, $Re = 100$, $\gamma = 0^\circ$ and $\varphi = 0.05$. In a further step, a comparison of the average Nusselt number as a function of the Hartmann number has also been plotted in Fig. 3 under the same conditions mentioned above. It is clear from these figures that the isotherms and the average Nusselt number are almost similar.

Therefore, the results of this work show very good agreement with the reference Hussain and Ahmed [18].

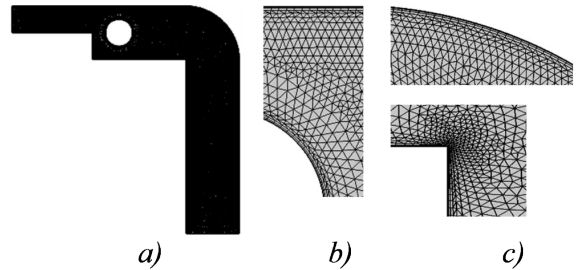


Fig. 2. Mesh: a) inside the computational domain, b) zoom near the cylinder, and c) zoom near the curvature

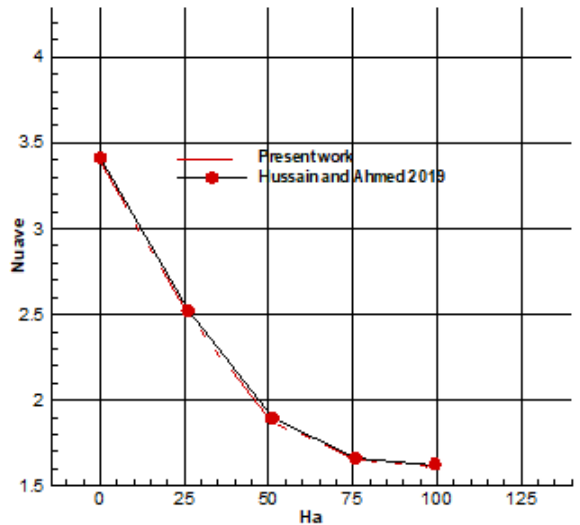


Fig. 3. Comparison of the Nusselt average as a function of Ha of the present study with the reference Hussain and Ahmed [21]

Table 5. The average number of Nusselt and temperature for several numbers of elements

Number of elements	17040	23713	31528	40401	50293	60970
Time of simulation [s]	17	25	30	50	55	78
Nu_{ave}	4.88585	4.89666	4.90630	4.92318	4.92170	4.92185
θ_{ave}	0.14977	0.15111	0.15257	0.15413	0.15424	0.15461
θ	0.05355	0.05361	0.05462	0.05530	0.05537	0.05534

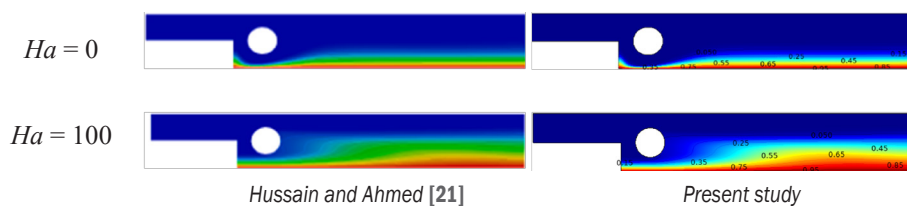


Fig. 4. Comparison of the isotherms of the present study with the reference the reference Hussain and Ahmed [21]

4 RESULTS AND DISCUSSIONS

In this section, the results of the numerical simulation of the nanofluid flow in a downward curved duct are shown. The isotherms, streamlines and average Nusselt number are presented for different values of Hartmann number Ha (0, 50, 100), Reynolds number Re (10, 100, 200), nanoparticle volume fraction φ (0 %, 5 %, 1 %) and magnetic field inclination angle γ (0° , 60° , 90°). The simulation was based on demonstrating for each value of the curvature angle g (0° , 30° , 45° , 60° , 90°) the effect of these control parameters on the thermo hydrodynamic nanofluid behavior. In this study, water is the basic fluid in the formation of ferrofluid with $Pr = 6.2$. On the other hand, the presentation of the different profiles and graphs consists in setting the Reynolds number,

the Hartmann number, the angle of inclination of the magnetic field and the volume fraction of the nanoparticles respectively to $Re = 300$, $Ha = 50$, $\gamma = 0^\circ$ and $\varphi = 0.05$ when the influence of one of them is highlighted.

4.1 Effect of Hartmann number

Fig. 5 gives the influence of the Hartmann number on the streamlines at different curvature angles. In the absence of the magnetic field for a straight geometry ($g = 90^\circ$), an equilibrium between the pressure gradient and the centrifugal force is established downstream of the cylinder, so the action of the centrifugal and viscous forces simultaneously leads to the appearance of two counter-rotating vortices in the downstream part of the cylinder. Furthermore, by increasing

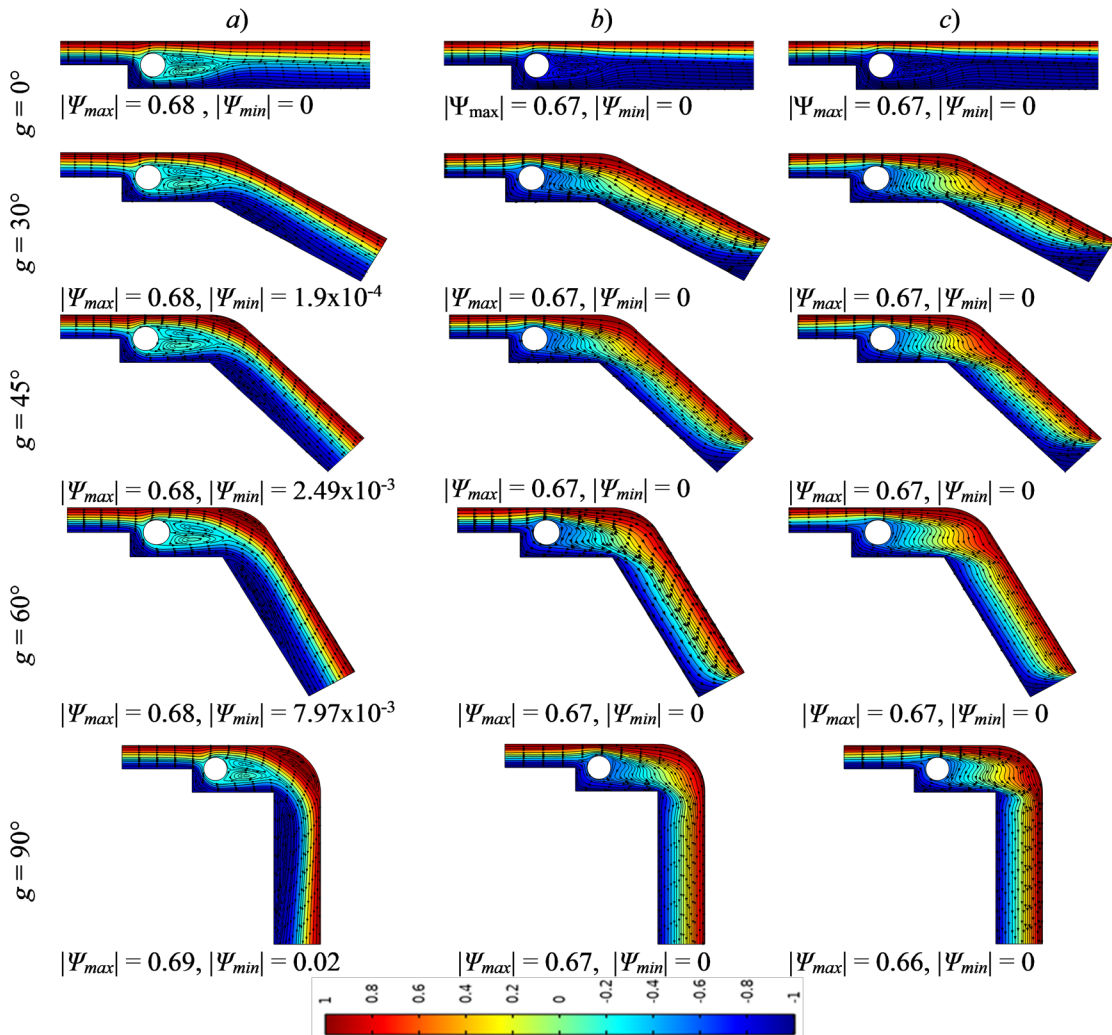


Fig. 5. Streamlines at different angles of curvature (g) for a) $Ha = 0$, b) $Ha = 50$, and c) $Ha = 100$, when $Pr = 6.2$.

duct curvature angle g (30° , 45° , 60°) again in the absence of the magnetic field $Ha = 0$, we observe the formation of recirculation zones which are in this case dead zones, especially in the immediate vicinity of the curved hot wall, these vortices tend to widen by increasing the angle of curvature. As the magnetic field intensity increases from $Ha = 0$ to $Ha = 100$, these vortices disappear, favoring the contact of the ferrofluid with the hot wall. The increase in magnetic field intensity in the case of a straight duct ($g = 0^\circ$) leads to an opposite impact to that of a curved duct. The mobility of nanoparticles in the duct decreases in terms of current function and velocity magnitude with increasing magnetic field in the case of a straight duct geometry ($g = 0^\circ$), in contrast to a curved duct the flow intensifies with increasing Hartmann number. This behaviour is due to the Lorentz force, which obstructs the ferrofluid in the first case and drives it in the second case. The magneto hydrodynamic behaviour has an effect on the temperature contours as shown in Fig. 6. In fact, the intensity of forced convection

increases as the Hartmann number increases from $Ha = 0$ (without magnetic field) to $Ha = 100$ in curved duct case g (30° , 45° , 60° , 90°). A reduction of the thermal boundary layer has been noted by virtue of the good heat transfer. Therefore the Nusselt number is better in straight curvature angle case $g = 90^\circ$ on the one hand. On the other hand, in a straight duct case, the convection decreases by increasing the Hartmann number, the lines of the isotherms start to move towards the adiabatic wall at the top so the thermal boundary increases. Fig. 7 illustrates the effect of the curvature angle on the local Nusselt number along the hot wall in the case of Hartmann number values $Ha = 0$ and $Ha = 100$ respectively. It was found that in the absence of the magnetic field ($Ha = 0$), the local Nusselt number marks an increase in the initial part of the hot wall (just below the cylinder), so with the increase of the curvature angle it is found that the local Nusselt number decreases. Moreover in the case of a strong magnetic field ($Ha = 100$) the local Nusselt number shows an increase in the initial part of

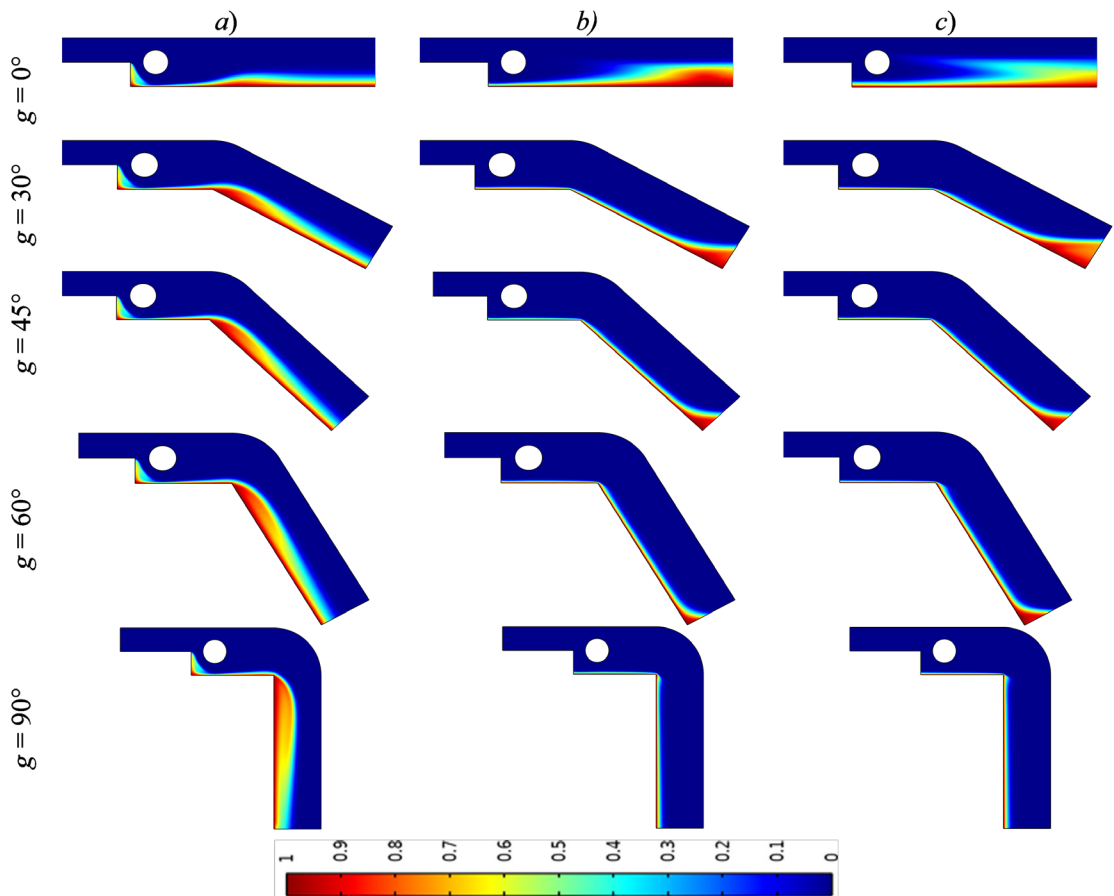


Fig. 6. Isotherms at different angles of curvature (g) for a) $Ha = 0$, b) $Ha = 50$, and c) $Ha = 100$

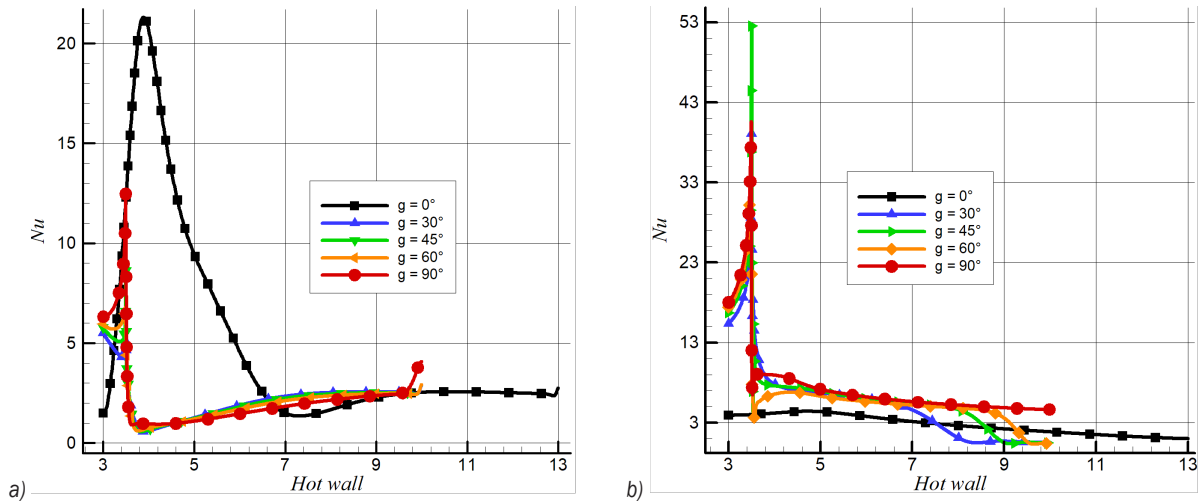


Fig. 7. The effect of the curvature angle around the hot wall on local Nusselt: a) $Ha = 0$, and b) $Ha = 100$

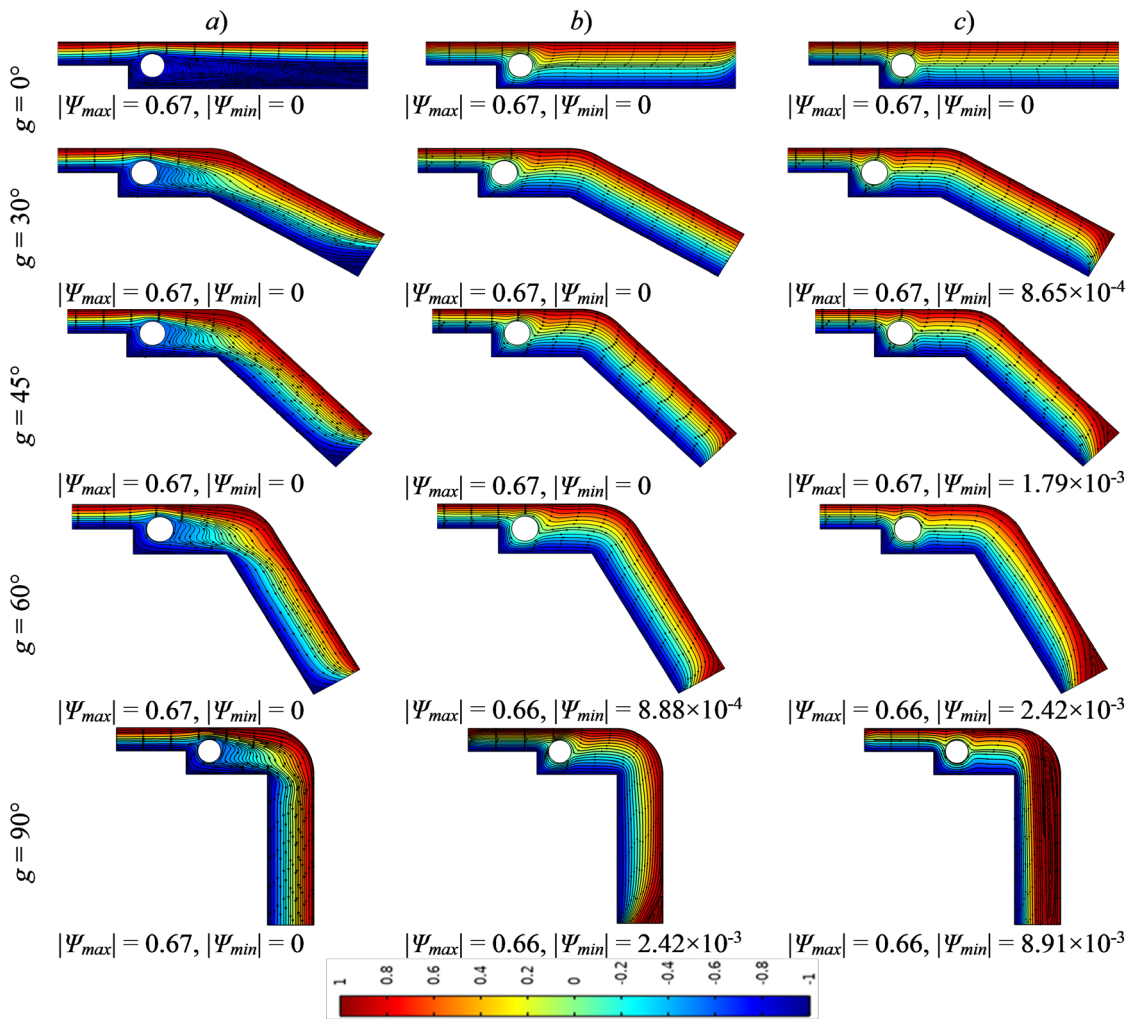


Fig. 8. Streamlines at different angles of curvature (g) for: a) $\gamma = 0^\circ$, b) $\gamma = 60^\circ$, and c) $\gamma = 90^\circ$

the curvature hot wall part. Indeed the increase of the curvature angle leads to an improvement of the local Nusselt number in the curvature part.

This behavior is due to the Lorentz force that drives the flow in the curved part.

4.2 The Effect of the Inclination Angle of the Magnetic Field

Fig. 8 shows the hydrodynamic behavior of the nanofluid for different magnetic field inclination angles. It has been observed that in the case of straight duct ($g = 0^\circ$), the ferrofluid flow is slow at the bottom of the cylinder at horizontal magnetic field ($\gamma = 0^\circ$). Therefore by increasing the magnetic field inclination, the mobility of the nanoparticles increases to its maximum at the bottom in the vicinity of the cylinder near the hot wall at a vertical magnetic field ($\gamma = 90^\circ$). Moreover, a mobility was noted in terms of current

function in the curved part by increasing the duct curvature angle of g ($30^\circ, 45^\circ, 90^\circ$) in the presence of a horizontal magnetic field. In contrast, in the presence of a vertical magnetic field and increasing the curvature angle, the current function lines are almost identical except in the case of curvature angle $g = 90^\circ$, where the nanofluid flow marks a significant recirculation region at zero velocities in the immediate vicinity of the adiabatic wall. Physically this phenomenon is by virtue of the Lorentz force, which is driving as we increase the angle of inclination of the magnetic field from $0^\circ, 60^\circ$ to 90° where we note a strong flow in the case of a straight duct. On the other hand, the increase in the angle of inclination of the magnetic field directs this force in direction that obstructs the flow in the case of a curved for all angles of curvature. The isotherms presented in Fig. 9 show the thermal behavior, which is strongly influenced by the hydrodynamic state of the nanofluid under the

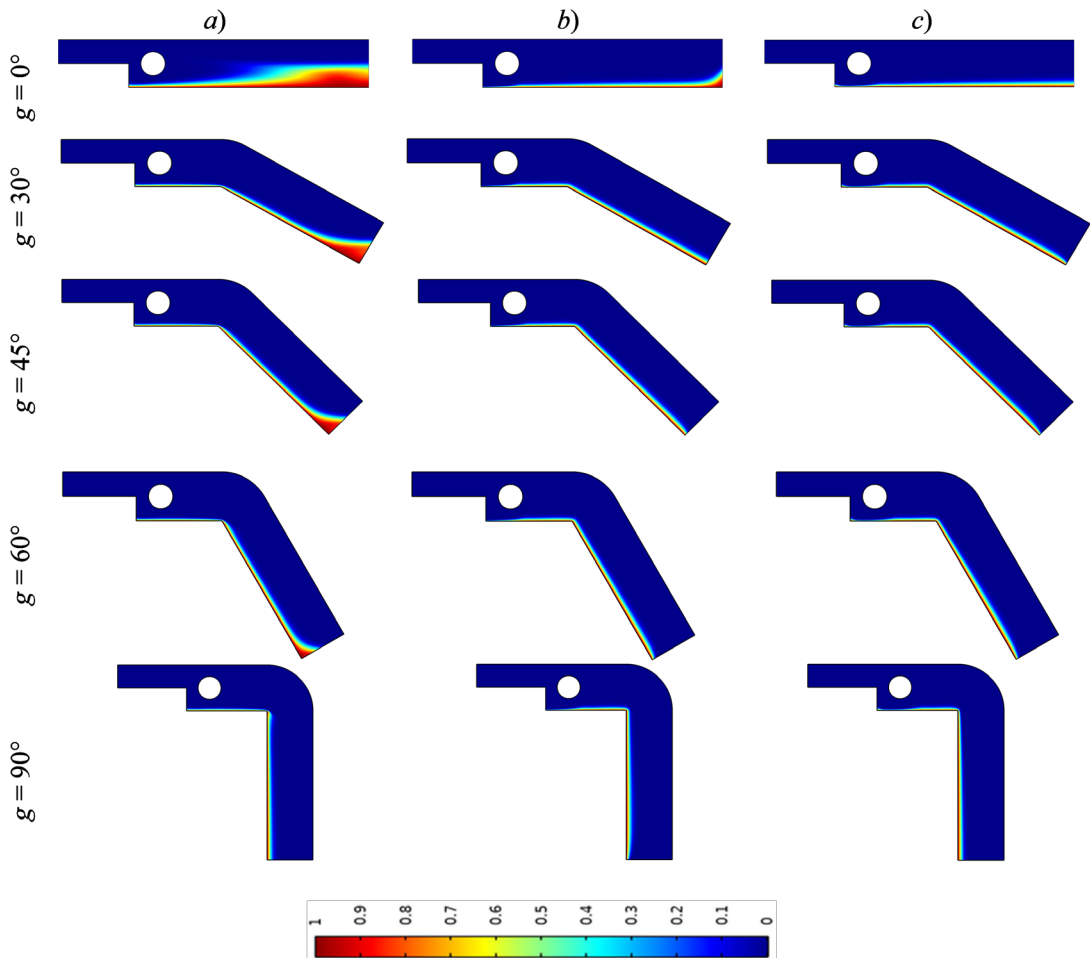


Fig. 9. Isotherms at different angles of curvature (g) for: a) $\gamma = 0^\circ$, b) $\gamma = 60^\circ$, and c) $\gamma = 90^\circ$

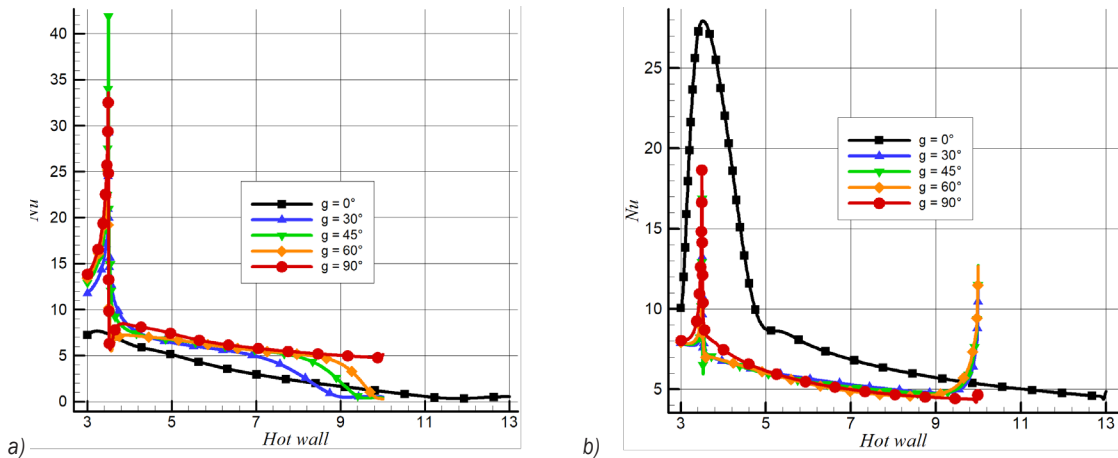


Fig. 10. The effect of the curvature angle around the hot wall on local Nusselt number: a) at horizontal magnetic field ($\gamma = 0^\circ$), and b) at a vertical magnetic field ($\gamma = 90^\circ$)

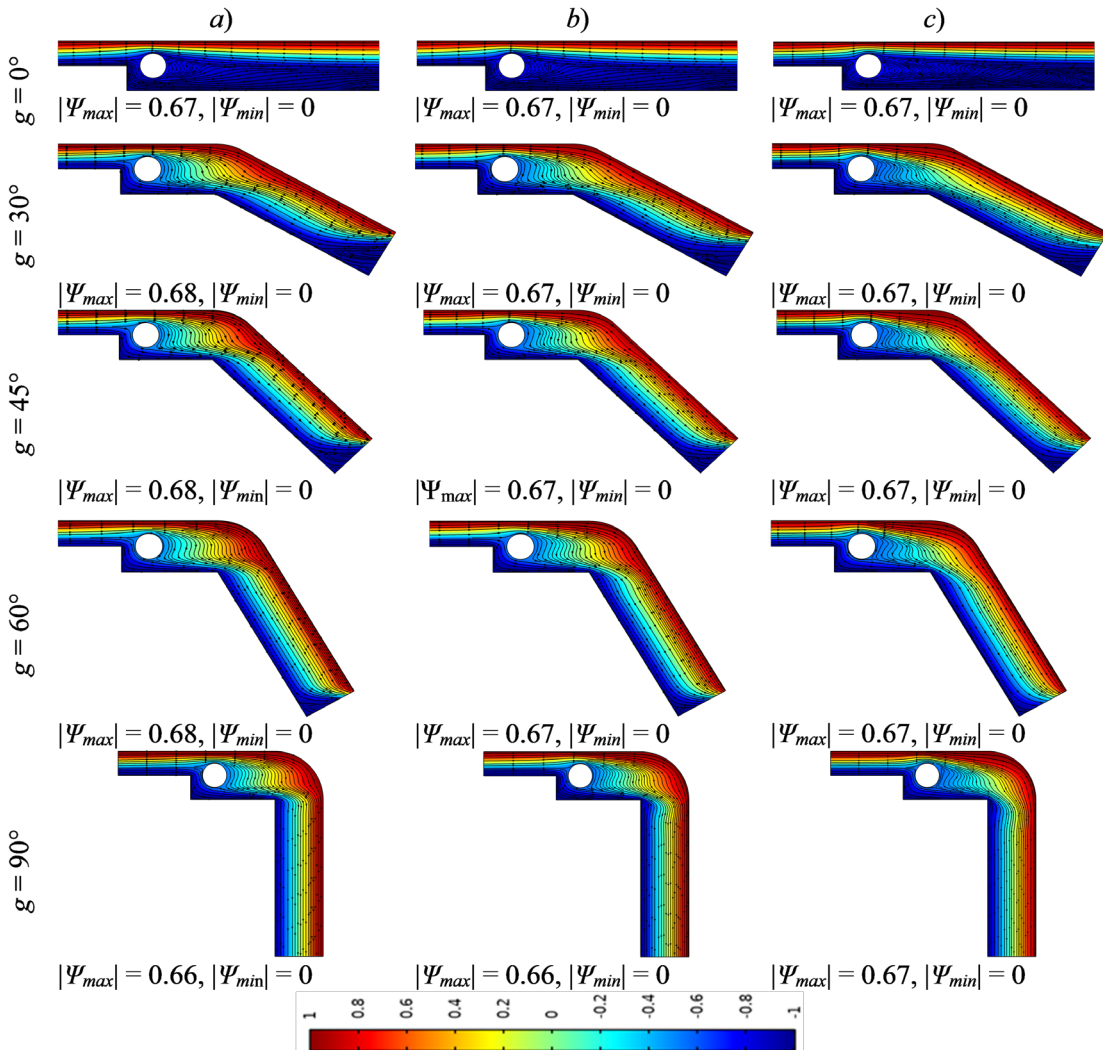


Fig. 11. Streamlines at different angles of curvature (g) for: a) $Re = 10$, b) $Re = 100$, and c) $Re = 300$

effect of the magnetic field inclination angle. In the case of a horizontal magnetic field, a decrease of the thermal layer is underlined in the case of a straight duct as the magnetic field inclination angle increases. Indeed, a reduced thermal layer corresponding to a good thermal convection is observed for a vertical magnetic field ($\gamma = 90^\circ$). On the other hand, for a horizontal field by increasing the curvature angle, the thermal layer is reduced in the curved part due to the good thermal transfer. Moreover, by increasing the angle of curvature, the increase of the angle of inclination of the magnetic field has no effect on the heat transfer. Fig. 10 shows the variation of the local Nusselt number along the hot wall for the two values of inclination angle respectively $\gamma = 0^\circ$ and $\gamma = 90^\circ$. We observe an improved local Nusselt number in the curved part in the case of a horizontal inclination angle ($\gamma = 0^\circ$). On the other hand in the case of a vertical inclination angle ($\gamma = 90^\circ$) the local Nusselt

number in the curved part is practically the same by increasing the curvature angle and in the straight part, it increases relatively.

4.3 The Effect of Reynolds Number

Fig. 11 shows the influence of Reynolds number (or inertia) on the streamlines of the Fe_2O_3 -water nanofluid flow in the downward curved duct. A significant increase in Reynolds number from a value of 10 to a value of 300, leads to significant changes in the hydrodynamic behavior of the nanofluid flow. In fact, in the case of a straight duct, the flow becomes more intensity as the Reynolds number increases, thus favoring the attachment of the nanofluid due to the enlarged duct type used. Furthermore, by increasing the curvature angle of the duct as well as the Reynolds number, the flow of the nanofluid becomes stronger where it marks its intensity at a curvature angle (g

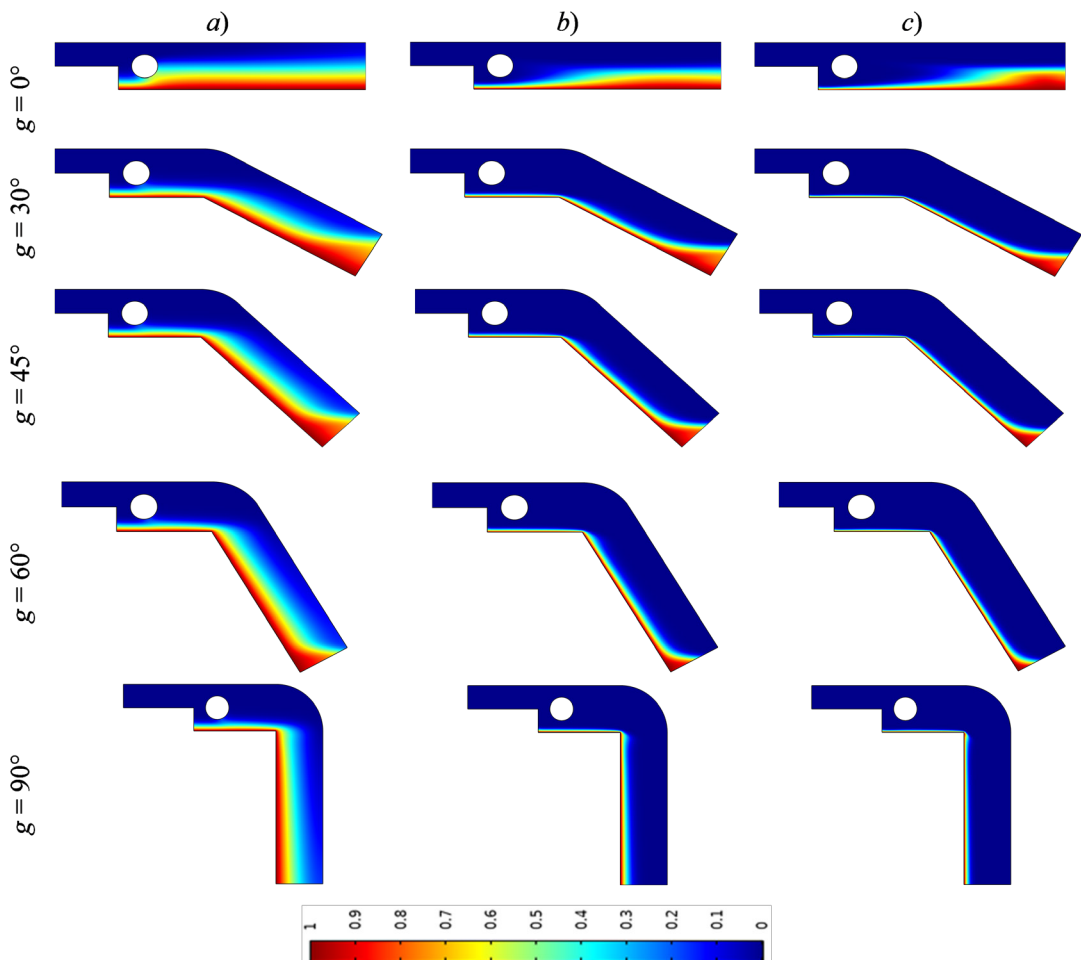


Fig. 12. Isotherms at different angles of curvature (g) for: a) $Re = 10$, b) $Re = 100$, and c) $Re = 300$

= 90°) thus favoring the attachment at a Reynolds number (Re = 300). This phenomenon is due on the one hand to the inertial forces which predominate the viscous forces as well as the Lorenz force when the Reynolds number increases in the case of a horizontal curvature angle ($g = 0^\circ$). Moreover, by increasing the angle of curvature, the viscous forces and the Lorenz force carry away the flow next to the inertia forces, which increase with the increase of the Reynolds number. The thermal behavior is strongly influenced by the hydrodynamic state of the nanofluid under the effect of the inertia as shown in Fig. 12. Indeed the thermal band marks a decrease with the increase of the inertia in the case of a straight duct. On the other hand, we note a decrease of the thermal layer, which extends towards the hot wall increasingly by

raising simultaneously the angle of curvature and the Reynolds number, reflecting an improved thermal transfer. Moreover, a significantly reduced thermal layer is mentioned in the case of a curvature angle ($g = 90^\circ$) for a Reynolds number (Re = 300), by virtue of a good convection that took place in this situation.

4.4 Effect of Nanoparticle Concentration

Fig. 13 shows the streamline profiles for different curvature angles at different average nanoparticle concentrations φ (0, 0.05, 0.1).

It can be seen from this figure that there is no change in the streamline pattern by adding nanoparticles at different volume fractions to the base fluid. This is due on the one hand to the use of particles

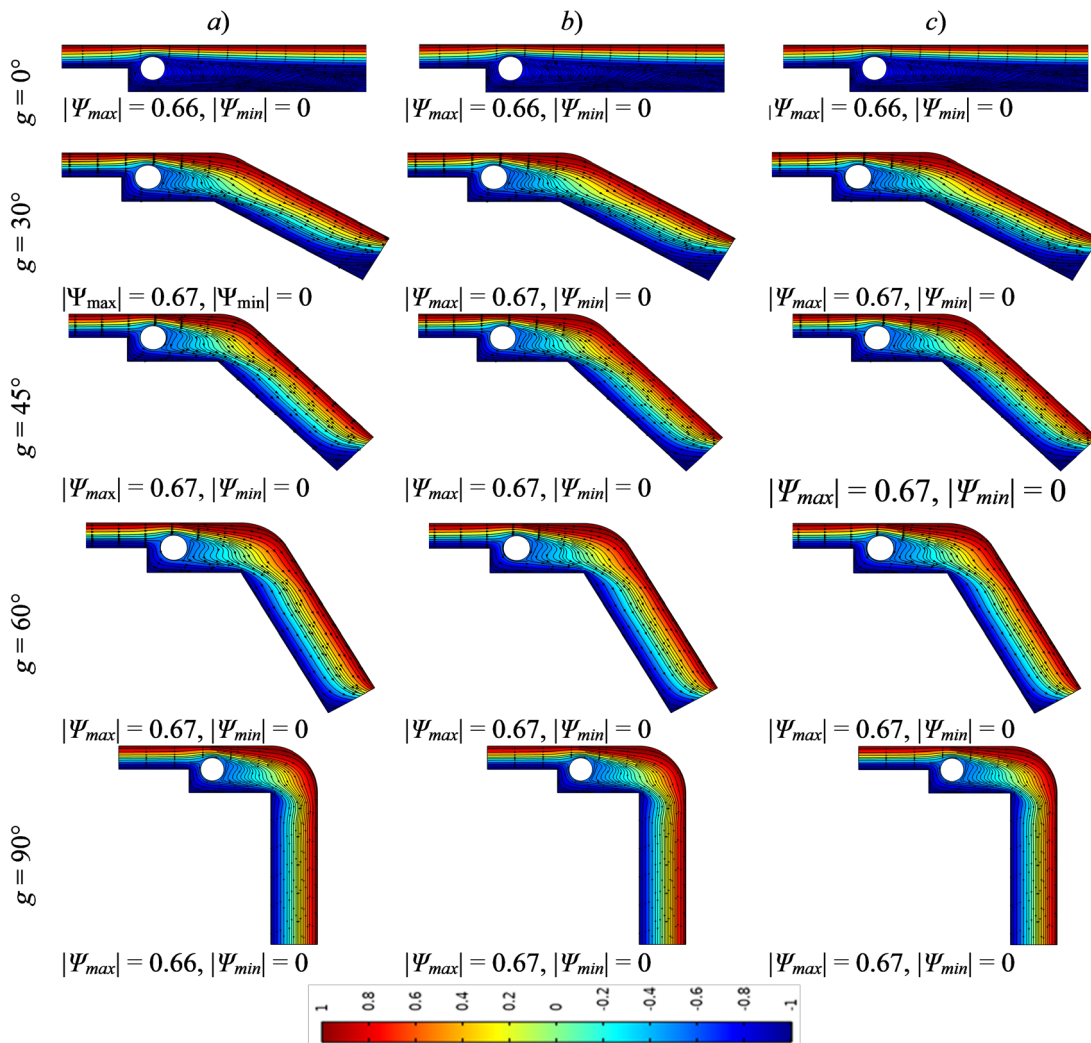


Fig. 13. Streamlines at different angles of curvature (g) for: a) $\varphi = 0$, b) $\varphi = 0.05$, and c) $\varphi = 0.1$.

of nanometric diameters at low concentrations. On the other hand, the injection of nanoparticles in applications related to heat transfer. In fact, the absence of buoyancy force based on the conditions of this study (forced convection) does not show the influence of the temperature formerly affected by the presence of nanoparticles on the hydrodynamic behavior. Indeed a weak influence of the viscosity and density on this behavior. From Fig. 14, it appears that the isotherms profiles show similarly no change. With the increase of the concentration of nanoparticles, the temperature increases in the middle of the duct in the straight part as well as the curved part. Indeed, a good increase is marked in the case of a curvature angle ($g = 90^\circ$) and a nanoparticle concentration $\varphi = 0.1$, see Fig. 15. Effectively the increase of the temperature

of the cold medium leads to a reduction in terms of thermal gradient.

4.5 Effect of Hartmann Number on Nusselt Number

The profiles of the average Nusselt number for different Hartmann numbers are shown in Fig. 16a. Indeed at an angle of a horizontal magnetic field ($\gamma = 0^\circ$), the Lorenz force obstructs the flow in the case of a straight duct ($g = 0^\circ$) due to the perpendicularity between them.

Moreover, the increase of the magnetic field disfavors the forced convection, which explains the reduction of the mean Nusselt number by increasing the Hartmann number. In contrast, for a curved duct g ($30^\circ, 45^\circ, 60^\circ, 90^\circ$) the increase of the Hartmann

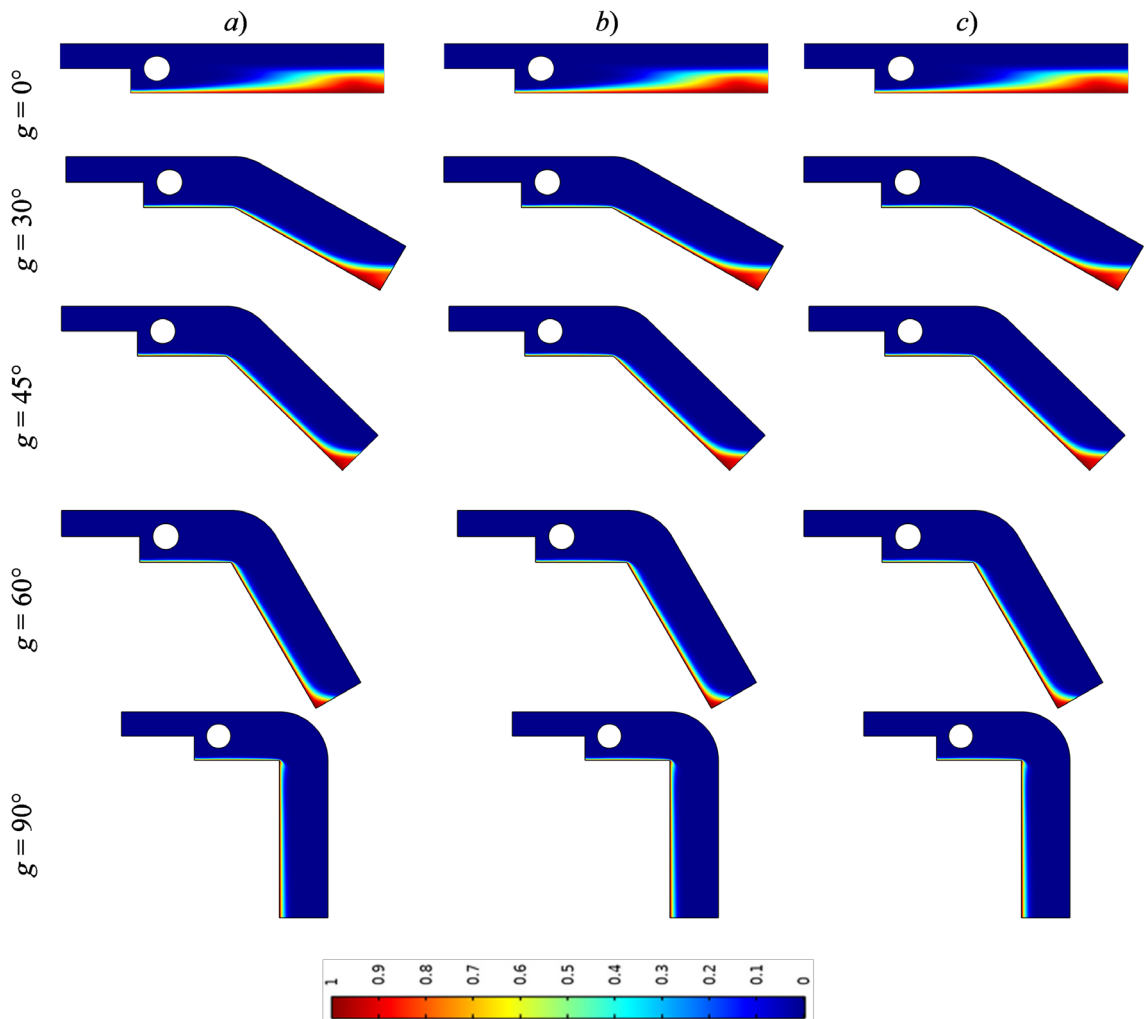


Fig. 14. Isotherms at different angles of curvature (g) for: a) $\varphi = 0$, b) $\varphi = 0.05$, and c) $\varphi = 0.1$

number as well as the curvature angle marks an increase of the average Nusselt number which achieves its maximum in the case of a curvature angle $g = 90^\circ$. This behavior is in virtue of the magnetic force that drives the ferrofluid flow at latter case. Thus, a decrease of the thermal boundary layer was noted in this case. Overall the increase in the average heat transfer rate throughout the system reaches about 240.74 % when the Hartmann number increases from 0 to 100 at curvature angle $g = 90^\circ$.

4.6 Effect of the Magnetic Field Inclination Angle on the Nusselt Number

Fig. 16b shows the average Nusselt number profiles at different curvature angles. It can be seen that the

direction of the magnetic field significantly affects the average Nusselt number by increasing the curvature angle. Thus, an improvement of the average Nusselt number was noted with the increase of the magnetic field angle and the curvature angle except in the case of a vertical magnetic field ($\gamma = 90^\circ$) where the increase of the curvature angle does not show any effect. This is in contrast to the case of a straight duct where the increase in the inclination of the magnetic field promotes heat transfer. Moreover, in the cases of curvature angles g ($30^\circ, 45^\circ, 60^\circ, 90^\circ$), the vertical magnetic field increases the average Nusselt number in the duct straight part and decreases it in its curved part.

Physically, this behavior is due to the Lorenz force that drives the flow in the first part. In the

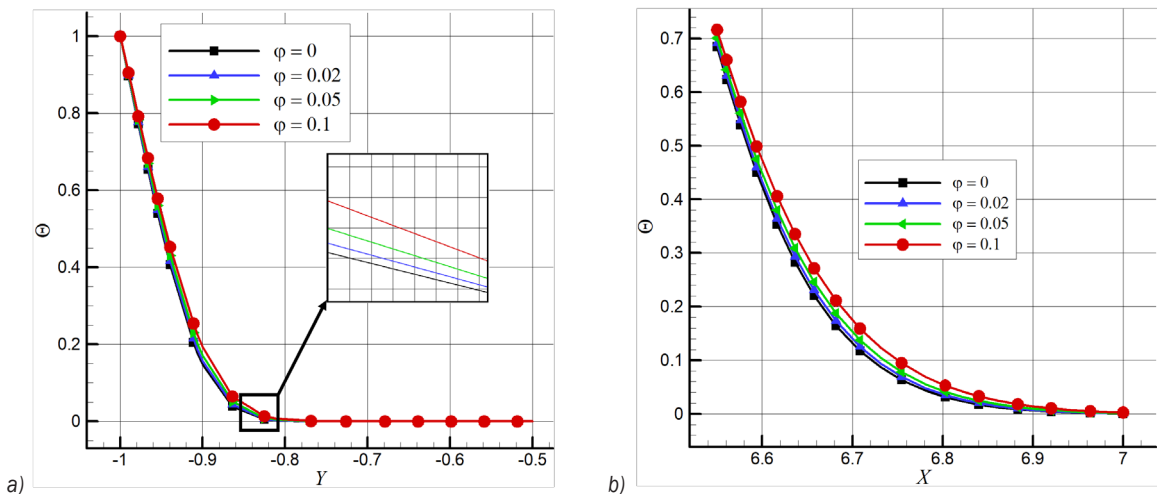


Fig. 15. Dimensionless temperature component for different volume fractions (ϕ) at curvature angle ($g = 90^\circ$) for: a) along the vertical line $X = 5, Y = -1$, and b) along the horizontal line $X = 6.55, Y = -3$

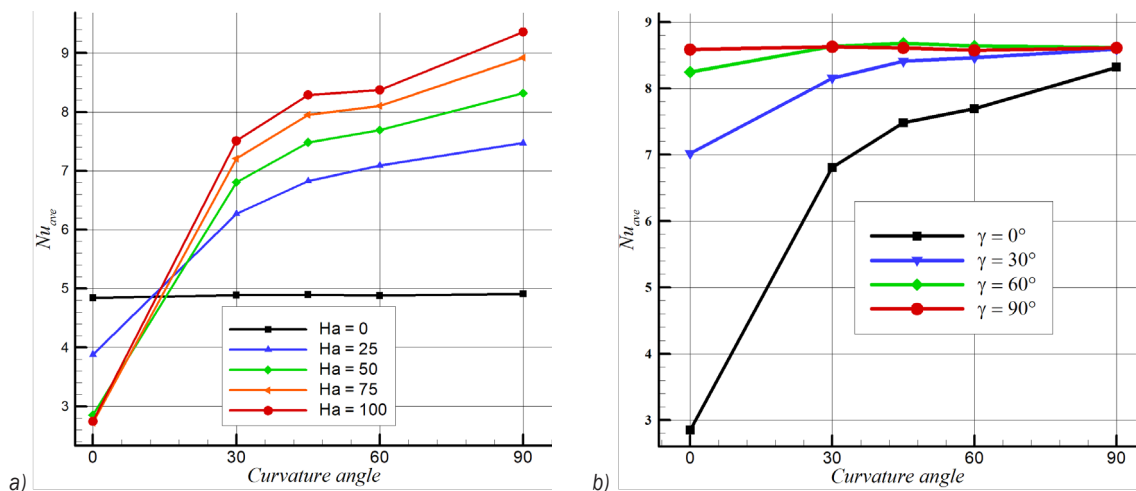


Fig. 16. Effect on average Nusselt number at different curvature angle (g) of: a) Hartman number (Ha), and b) the magnetic field inclination (γ)

second part, i.e. the curved part, as the curvature angle increases, the Lorenz force acts so that the ferrofluid moves away from the hot wall, thus disfavoring the thermal transfer. Indeed, on the one hand by increasing the curvature angle in the case of horizontal magnetic field, the heat transfer rate increase of 191.95 % has been noted at a curvature angle ($g = 90^\circ$). On the other hand in the case of a vertical magnetic field the heat transfer is not significantly affected by the curvature angle increase, were we note the heat transfer rate increase of 0.31 % at an angle of curvature ($g = 90^\circ$).

4.7 Effect of Reynolds NUMBER on Nusselt Number

Fig. 17a shows the variation of the average Nusselt number with increasing Reynolds number. In the case of a straight duct the average Nusselt number increases with increasing Reynolds number. Indeed the forced convection is improved as the Reynolds number increases. This behavior is explained by the predominance of inertial forces over viscosity forces. Moreover, the convection is better at high Reynolds numbers in the case of a curved duct. This phenomenon is due to the viscosity forces, which are damped as the curvature angle increases. As a result, the average Nusselt number increases to its maximum for a Reynolds number value $Re = 300$ in the case of a right curvature angle ($g = 90^\circ$).

Thus, the heat transfer is improved. Indeed, it was recorded an increase of the Nusselt number from the value of 0.90 to the value of 2.85 with an increase in the thermal rate of almost 214.62 % following an increase of the Reynolds number from 10 to 300 in the

case of a straight duct. Furthermore, by increasing the curvature angle, it was found that the average Nusselt number increased from 1.80 to 8.32 with an increase in the heat transfer rate of 362.77 % at a curvature angle ($g = 90^\circ$).

4.8 Effect of Nanoparticle Concentration on Nusselt Number

The variation of the heat exchange rate with the nanofluid use is an objective consideration for all applications including this type of heat transfer fluid. The average Nusselt number distribution shown in Fig. 17b obviously shows that the heat rate increases with increasing nanoparticle concentration and with increasing curvature angle. Moreover, an improvement in heat transfer at a curvature angle ($g = 90^\circ$) of up to 12.5 % is recorded with the use of nanofluid with a concentration of 0.1 compared to the pure water.

5 CONCLUSIONS

In the present numerical study, the magnetohydrodynamic behavior of forced convection of a laminar $Fe_3O_4-H_2O$ flow in a backward facing curved duct comprising a fixed cylinder has been investigated. The governing equations solved by the finite element method and wide control parameters ranges have been considered. Hence, the effects of Hartmann number, Reynolds number, magnetic field inclination angle and nanoparticle concentration on the thermo-magnetohydrodynamic nanofluid behavior

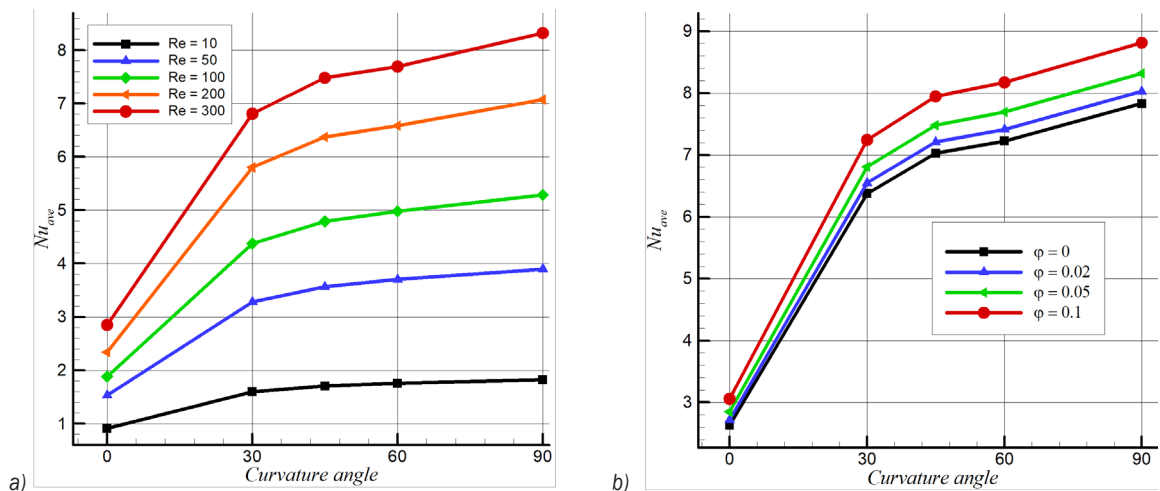


Fig. 17. Effect on average Nusselt number at different curvature angle (g) of: a) the Reynolds number (Re), and b) the nanoparticle volume fraction (ϕ)

have been demonstrated. Through this study, the following essential points have been demonstrated:

- The increase in the Hartmann number slows down the ferrofluid flow within the straight duct with a backward facing step. However, this increase in the Hartmann number decreases the average Nusselt number in the straight duct case. On the other hand, the increase of the curvature angle as well as the magnetic field intensity favors the heat transfer. Therefore, the average Nusselt number improves by reaching its maximum value at the right curvature angle.
- The increase in the inclination angle degree of the magnetic field affects positively the heat transfer in the case of a straight duct with a backward facing step. Indeed this increase improves the average Nusselt number in this case. Moreover, the rise of the curvature angle as well as the magnetic field angle increases the convective heat transfer except for the straight magnetic field where the curvature angle shows no effect on the heat transfer.
- The increase in the Reynolds number leads to a significant enhancement of the convective heat transfer. In addition, with the increase of the curvature angle dampens the effect of viscous forces, thus, promoting heat transfer even more.
- The addition of Fe_3O_4 nanoparticles to pure water improves the heat transfer. In this case, the value of the average Nusselt number increases by almost 12.5 % compared to the pure water used. However, due to the low concentrations introduced, the nanofluid hydrodynamic was not largely affected due to low concentrations used.

7 NOMENCLATURE

C_p	specific heat [$\text{J}\cdot\text{kg}^{-1}\cdot\text{K}^{-1}$]
K	thermal conductivity [$\text{W}\cdot\text{m}^{-1}\cdot\text{K}^{-1}$]
Ha	Hartmann number
q	heat flux density [$\text{W}\cdot\text{m}^{-2}$]
Re	Reynolds number
Nu_{ave}	average Nusselt number
Nu	local Nusselt number
Pr	Prandtl number
P	pressure [Pa]
P_{atm}	atmospheric pressure [Pa]
x, y	Cartesian coordinates [m]
X, Y	dimensionless coordinates
g	curvature angle [$^\circ$]
H	step height
T	temperature [K]

T_c	cold temperature [K]
T_h	hot temperature [K]
u	velocity in x direction [$\text{m}\cdot\text{s}^{-1}$]
v	velocity in y direction [$\text{m}\cdot\text{s}^{-1}$]
V, U	Dimensionless velocity
\bar{u}	Vertical wall velocity [$\text{m}\cdot\text{s}^{-1}$]

Greek symbols

α	thermal diffusivity [$\text{m}^2\cdot\text{s}^{-1}$]
β	thermal expansion coefficient [K^{-1}]
θ	dimensionless local temperature
μ	dynamic viscosity [$\text{kg}\cdot\text{m}^{-1}\cdot\text{s}^{-1}$]
ρ	density [$\text{kg}\cdot\text{m}^{-3}$]
σ	electrical conductivity [$\Omega^{-1}\cdot\text{m}^{-1}$]
γ	magnetic field inclination angle
φ	volume fraction
θ_{ave}	dimensionless average temperature

Subscripts:

s	solid
c	cold
f	base fluid
h	hot
ff	ferro-fluid
p	nanoparticles

8 REFERENCES

- [1] Erturk, E. (2008). Numerical solutions of 2-D steady incompressible flow over a backward-facing step, Part I: High Reynolds number solutions. *Computers & Fluids*, vol. 37, no. 6, p. 633-655, DOI:10.1016/j.compfluid.2007.09.003.
- [2] Lan, H., Armaly, B.F., Drallmeier, J.A. (2009). Three-dimensional simulation of turbulent forced convection in a duct with backward-facing step. *International Journal of Heat and Mass Transfer*, vol. 52, no. 7-8, p. 1690-1700, DOI:10.1016/j.ijheatmasstransfer.2008.09.022.
- [3] Iwai, H., Nakabe, K., Suzuki, K. (2000). Flow and heat transfer characteristics of backward-facing step laminar flow in a rectangular duct. *International Journal of Heat and Mass Transfer*, vol. 43, no. 3, p. 457-471, DOI:10.1016/S0017-9310(99)00140-4.
- [4] Star, S., Stabile, G., Rozza, G., Degroote, J. (2021). A POD-Galerkin reduced order model of a turbulent convective buoyant flow of sodium over a backward-facing step. *Applied Mathematical Modelling*, vol. 89, p. 486-503, DOI:10.1016/j.apm.2020.07.029.
- [5] Kahine, K., Nguyen, V.T., Lebouché, M. (1997). Non-Newtonian Flow through Enlargements. *International Communications in Heat and Mass Transfer*, vol. 24, no. 8, p. 1103-1112, DOI:10.1016/S0735-1933(97)00104-8.
- [6] Mahmood, R., Bilal, S., Majeed, A.H., Khan, I., Sherif, E.S.M. (2020). A comparative analysis of flow features of Newtonian and power law material: a New configuration. *Journal of Materials Research and Technology*, vol. 9, no. 2, p. 1978-1987, DOI:10.1016/j.jmrt.2019.12.030.

- [7] Dejoan, A., Leschziner, M.A. (2004). Large eddy simulation of periodically perturbed separated flow over a backward-facing step. *International Journal of Heat and Fluid Flow*, vol. 25, no. 4, p. 581-592, DOI:10.1016/j.ijheatfluidflow.2004.03.004.
- [8] Benard, N., Sujar-Garrido, P., Bonnet, J.P., Moreau, E. (2016). Control of the coherent structure dynamics downstream of a backward facing step by DBD plasma actuator. *International Journal of Heat and Fluid Flow*, vol. 61, p. 158-173, DOI:10.1016/j.ijheatfluidflow.2016.04.009.
- [9] Li, Z.Y., Guo, S., Bai, H.L., Gao, N. (2019). Combined flow and heat transfer measurements of backward facing step flows under periodic perturbation. *International Journal of Heat and Mass Transfer*, vol. 130, p. 240-251, DOI:10.1016/j.ijheatmasstransfer.2018.10.077.
- [10] Koide, Y., Sasaki, R., Kameya, Y., Motosuke, M. (2015). A burst wave-induced plasma actuator for controlling separated flow over a backward-facing step at low Reynolds numbers. *Experimental Thermal and Fluid Science*, vol. 66, p. 72-78, DOI:10.1016/j.expthermflusci.2015.03.016.
- [11] Tihon, J., Pěnkavová, V., Pantzali, M. (2010). The effect of inlet pulsations on the backward - facing - step flow. *European Journal of Mechanics B/Fluids*, vol. 29, no. 3, p. 224-235, DOI:10.1016/j.euromech-b.2010.02.001.
- [12] Mohamed, H., Camdali, U., Biyikoglu, A., Aktas, M. (2022). Enhancing the Performance of a Vapour Compression Refrigerator System Using R134a with a CuO/CeO₂ Nano-refrigerant. *Strojniški vestnik - Journal of Mechanical Engineering*, vol. 68, no. 6, p. 395-410, DOI:10.5545/sv-jme.2021.7454.
- [13] Al-Kouz, W. G., Kiwan, S., Alkhalidi, A., Sari, M. E., & Alshare, A. (2018). Numerical study of heat transfer enhancement for low-pressure flows in a square cavity with two fins attached to the hot wall using Al₂O₃-air nanofluid. *Strojniški vestnik - Journal of Mechanical Engineering*, vol. 64, no. 1, p. 26-36, DOI:10.5545/sv-jme.2017.4989.
- [14] Taamneh, Y., & Bataineh, K. (2017). Mixed convection heat transfer in a square lid-driven cavity filled with Al₂O₃-water nanofluid. *Strojniški vestnik - Journal of Mechanical Engineering*, vol. 63, no. 6, p. 383-394, DOI:10.5545/sv-jme.2017.4449.
- [15] Selimefendigil, F., Öztop, H.F. (2013). Identification of forced convection in pulsating flow at a backward facing step with a stationary cylinder subjected to nanofluid. *International Communications in Heat and Mass Transfer*, vol. 45, p. 111-121, DOI:10.1016/j.icheatmasstransfer.2013.04.016.
- [16] Hilo, A.K., Iborra, A.A., Sultan, M.T.H., Hamid, M.F.A. (2020). Experimental study of nanofluids flow and heat transfer over a backward facing step channel. *Powder Technology*, vol. 372, p. 497-505, DOI:10.1016/j.powtec.2020.06.013.
- [17] Togun, H., Safaei, M.R., Sadri, R., Kazi, S.N., Badarudin, A., Hooman, K., Sadeghinezhad, E. (2014). Numerical simulation of laminar to turbulent nanofluid flow and heat transfer over a backward-facing step. *Applied Mathematics and Computation*, vol. 239, p. 153-170, DOI:10.1016/j.amc.2014.04.051.
- [18] Ahmed, H.E., Kherbeet, A.S., Ahmed, M.I., Salman, B.H. (2018). Heat transfer enhancement of microscale backward facing step channel by using turbulators. *International Journal of Heat and Mass Transfer*, vol. 126, p. 963-973, DOI:10.1016/j.ijheatmasstransfer.2018.05.082.
- [19] Abbassi, H., Nassrallah, S.B. (2007). MHD flow and heat transfer in a backward-facing step. *International Communications in Heat and Mass Transfer*, vol. 34, no. 2, p. 231-237, DOI:10.1016/j.icheatmasstransfer.2006.09.010.
- [20] Kumar, A., Dhiman, A.K. (2012). Effect of a circular cylinder on separated forced convection at a backward facing step. *International Journal of Thermal Sciences*, vol. 52, p. 176-185, DOI:10.1016/j.ijthermalsci.2011.09.014.
- [21] Hussain, S., Ahmed, S.E. (2019). Unsteady MHD forced convection over a backward facing step including a rotating cylinder utilizing Fe₃O₄-water ferrofluid. *Journal of Magnetism and Magnetic Materials*, vol. 484, p. 356-366, DOI:10.1016/j.jmmm.2019.04.040.
- [22] Selimefendigil, F., Öztop, H.F. (2015). Influence of inclination angle of magnetic field on mixed convection of nanofluid flow over a backward facing step and entropy generation. *Advanced Powder Technology*, vol. 26, no. 6, p. 1663-1675, DOI:10.1016/j.jmmm.2019.04.040.
- [23] Mohammed, H.A., Fathinia, F., Vuthaluru, H.B., Liu, S. (2019). CFD based investigations on the effects of blockage shapes on transient mixed convective nanofluid flow over a backward facing step. *Powder Technology*, vol. 346, p. 441-451, DOI:10.1016/j.powtec.2019.02.002.
- [24] Kherbeet, A.S., Mohammed, H.A., Salman, B.H., Ahmed, H.E., Alawi, O.A. (2014). Experimental and numerical study of nanofluid flow and heat transfer over microscale backward-facing step. *International Journal of Heat and Mass Transfer*, vol. 79, p. 858-867, DOI:10.1016/j.ijheatmasstransfer.2014.08.074.
- [25] Lv, J., Hu, C., Bai, M., Li, L., Shi, L., Gao, D. (2019). Visualization of SiO₂-water nanofluid flow characteristics in backward-facing step using PIV. *Experimental Thermal and Fluid Science*, vol. 101, p. 151-159, DOI:10.1016/j.expthermflusci.2018.10.013.
- [26] Amiri, A., Arzani, H.K., Kazi, S.N., Chew, B.T., Badarudin, A. (2016). Backward-facing step heat transfer of the turbulent regime for functionalized graphene nanoplatelets based water-ethylene glycol nanofluids. *International Journal of Heat and Mass Transfer*, vol. 97, p. 538-546, DOI:10.1016/j.ijheatmasstransfer.2016.02.042.
- [27] Niemann, M., Fröhlich, J. (2016). Buoyancy-affected backward-facing step flow with heat transfer at low Prandtl number. *International Journal of Heat and Mass Transfer*, vol. 101, p. 1237-1250, DOI:10.1016/j.ijheatmasstransfer.2016.05.137.
- [28] Boruah, M.P., Pati, S., Randive, P.R. (2019). Implication of fluid rheology on the hydrothermal and entropy generation characteristics for mixed convective flow in a backward facing step channel with baffle. *International Journal of Heat and Mass Transfer*, vol. 137, p. 138-160, DOI:10.1016/j.ijheatmasstransfer.2019.03.094.
- [29] Selimefendigil, F., Öztop, H.F. (2013). Identification of forced convection in pulsating flow at a backward facing step with a stationary cylinder subjected to nanofluid. *International Communications in Heat and Mass Transfer*, vol. 45, p. 111-121, DOI:10.1016/j.icheatmasstransfer.2013.04.016.
- [30] Selimefendigil, F., Öztop, H.F. (2013). Numerical analysis of laminar pulsating flow at a backward facing step with an upper

- wall mounted adiabatic thin fin. *Computers & Fluids*, vol. 88, p. 93-107, DOI:10.1016/j.compfluid.2013.08.013.
- [31] Selimefendigil, F., Öztop, H.F. (2017). Forced convection and thermal predictions of pulsating nanofluid flow over a backward facing step with a corrugated bottom wall. *International Journal of Heat and Mass Transfer*, vol. 110, p. 231-247, DOI:10.1016/j.ijheatmasstransfer.2017.03.010.
- [32] Boruah, M.P., Randive, P.R., Pati, S. (2018). Hydrothermal performance and entropy generation analysis for mixed convective flows over a backward facing step channel with baffle. *International Journal of Heat and Mass Transfer*, vol. 125, p. 525-542, DOI:10.1016/j.ijheatmasstransfer.2018.04.
- [33] Mohammed, H.A., Alawi, O.A., Wahid, M.A. (2015). Mixed convective nanofluid flow in a channel having backward-facing step with a baffle. *Powder Technology*, vol. 275, p. 329-343, DOI:10.1016/j.powtec.2014.09.046.
- [34] Heshmati, A., Mohammed, H.A., Darus, A.N. (2014). Mixed convection heat transfer of nanofluids over backward facing step having a slotted baffle. *Applied Mathematics and Computation*, vol. 240, p. 368-386, DOI:10.1016/j.amc.2014.04.058.
- [35] Yanase, S.R.N.M., Mondal, R.N., Kaga, Y. (2005). Numerical study of non-isothermal flow with convective heat transfer in a curved rectangular duct. *International Journal of Thermal Sciences*, vol. 44, no. 11, p. 1047-1060, DOI:10.1016/j.ijthermalsci.2005.03.013.
- [36] Mondal, R.N., Islam, M.S., Uddin, M.K. (2013). Unsteady solutions with convective heat transfer through a curved duct flow. *Procedia Engineering*, vol. 56, p. 141-148, DOI:10.1016/j.proeng.2013.03.100.
- [37] Li, Y., Wang, X., Yuan, S., Tan, S.K. (2016). Flow development in curved rectangular ducts with continuously varying curvature. *Experimental Thermal and Fluid Science*, vol. 75, p. 1-15, DOI:10.1016/j.expthermflusci.2016.01.012.
- [38] Choi, H.K., Park, S.O. (1994). Mixed convection flow in curved annular ducts. *International Journal of Heat and Mass Transfer*, vol. 37, no. 17, p. 2761-2769, DOI:10.1016/0017-9310(94)90393-X.
- [39] Chandratilleke, T.T., Nadim, N., Narayanaswamy, R. (2012). Vortex structure-based analysis of laminar flow behaviour and thermal characteristics in curved ducts. *International Journal of Thermal Sciences*, vol. 59, p. 75-86, DOI:10.1016/j.ijthermalsci.2012.04.014.
- [40] Choi, J., Zhang, Y. (2012). Numerical simulation of laminar forced convection heat transfer of Al2O3-water nanofluid in a pipe with return bend. *International Journal of Thermal Sciences*, vol. 55, p. 90-102, DOI:10.1016/j.ijthermalsci.2011.12.017.
- [41] Ajeel, R.K., Sopian, K., Zulkifli, R., Fayyadh, S.N., Hilo, A.K. (2021). Assessment and analysis of binary hybrid nanofluid impact on new configurations for curved-corrugated channel. *Advanced Powder Technology*, vol. 32, no. 10, p. 3869-3884, DOI:10.1016/j.apt.2021.08.041.